Analyst

PAPER

View Article Online
View Journal

Cite this: DOI: 10.1039/c8an02139b

An aptamer based voltammetric biosensor for endotoxins using a functionalized graphene and molybdenum disulfide composite as a new nanocarrier

Yonghua Yuan,[a] Linlin Li,[a] Min Zhao,[b] Jing Zhou,[a] Zhihui Chen[a] and Lijuan Bai *[a]

Received 6th November 2018,
Accepted 22nd November 2018

DOI: 10.1039/c8an02139b

rsc.li/analyst

Lipopolysaccharides (LPS), known as endotoxins, can cause a strong inflammatory response and lead to multiple organ failure in severe cases. This work reports a simple label-free voltammetric aptasensor for highly sensitive determination of LPS using a polyethyleneimine (PEI) functionalized reduced graphene oxide (rGO) and molybdenum disulfide (MoS_2) composite (PEI-rGO-MoS_2) as a new nanocarrier for electroactive toluidine blue (TB). The PEI-rGO-MoS_2 nanocomposite with high electrical conductivity and large specific surface area can greatly increase the loading of TB and facilitate electron transfer from TB to an electrode. Then gold nanoparticles (AuNPs) were utilized to immobilize a thiolated LPS binding aptamer (LBA), which not only exhibited excellent biocompatibility, but also significantly amplified the electrochemical signal of TB. The proposed aptasensor exhibited high sensitivity for LPS and showed a wide linear range from 5.0×10^{-5} ng mL^{-1} to 2.0×10^{2} ng mL^{-1} with a low limit of detection (LOD) of 3.01×10^{-5} ng mL^{-1}, which overcame the shortcomings of traditional detection methods and achieved fast and accurate detection of LPS. Moreover, it exhibited excellent recovery and specificity upon spiking LPS in serum samples, indicating that this method has promising application in the field of trace analysis of LPS in clinical detection.

1. Introduction

Clinically, sepsis, endotoxemia and shock caused by Gram-negative bacteria (GNB) infection have a high mortality rate. Endotoxins, also referred to as lipopolysaccharides (LPS), are the major toxic components of GNB.[1] When the host organism is infected by GNB, LPS enter the bloodstream and cause a series of inflammatory reactions, which lead to multiple organ failure in severe cases. Due to the high toxicity of LPS, an extremely small amount of LPS can seriously threaten human life and health.[2] Therefore, the development of ultrasensitive methods for trace detection of LPS is of clinical significance.

At present, the most commonly used method for LPS detection is the semi-quantitative technique of *Limulus* amebocyte lysate (LAL) assay.[3] With regard to most enzymatic tests, the sensitive changes of pH and divalent cation concentrations in reagents can affect the accuracy of the target assay.[4] Along with the rapid development of detection technologies, a variety of quantitative test methods, such as turbidimetric assay,[5] modified matrix coloration method,[6] and enzyme-linked immunosorbent assay (ELISA),[7] have been explored to replace LAL as the main detection method for LPS. Compared with LAL, the above assays exhibit higher sensitivity and specificity. However, it should be noted that the shortcomings such as long time consumption, complicated operation procedure and need for expensive equipment may limit the wide application of these approaches in clinical testing. Therefore, searching for other more promising and desirable diagnostic techniques for LPS is imminent.[8]

Recently, biosensors based on LPS-specific substances,[9] such as cationic antibacterial proteins, binding proteins and peptides, especially aptamers, have been employed to detect LPS with excellent specificity, high sensitivity and a low limit of detection (LOD). Compared with an antigen–antibody recognition reaction, the binding of an aptamer to its target exhibits higher specificity and affinity, which frequently serves as an ideal recognition element for the fabrication of aptasensors.[10] Since the LPS binding aptamer (LBA) was synthesized by Choe's group,[11] it provides a new opportunity for LPS detection, while few studies have been reported using aptamer-

[a]*Engineering Technology Research Center for Pharmacodynamic Evaluation of Chongqing, College of Pharmacy, Chongqing Medical University, Chongqing 400016, PR China. E-mail: bailijua88@126.com; Fax: +86-023-68485161; Tel: +86-023-68485161*

[b]*Key Laboratory of Clinical Laboratory Diagnostics (Ministry of Education), College of Laboratory Medicine, Chongqing Medical University, Chongqing 400016, PR China*

based LPS biosensors.[12] In order to improve the detection performance, exploring novel nanomaterials with excellent stability and unique physicochemical properties that have broad applications in biosensors is highly desired.

Reduced graphene oxide (rGO) has attracted great attention in bioanalysis applications due to its high electrical conductivity, large specific surface area, favorable ductility and exceptional thermal stability.[13] For example, Rasheed and coworkers reported a DNA biosensor for breast cancer gene detection based on a rGO-yttria nanocomposite with high specificity.[14] On the other hand, molybdenum disulfide (MoS_2), a typical transition metal sulfide with a lamellar structure, is often employed as a matrix for biosensors because of its rich active edges and large specific surface area.[15] However, MoS_2 has a significant weakness of poor conductivity due to a serious accumulation phenomenon caused by its multi-layered structure.[16] In order to overcome this shortcoming, this work designed a polyethyleneimine (PEI) functionalized rGO and MoS_2 composite (PEI-rGO-MoS_2). The electrical conductivity of MoS_2 is dramatically promoted due to the p–n heterojunction formed by the strong coordination bond between rGO and MoS_2.[17] PEI is widely used in the field of electrochemical analysis because of its high conductivity and high water dispersibility. The addition of PEI increases the interlamellar spacing of rGO and MoS_2, making the PEI-rGO-MoS_2 composite have a better film formation and further increasing its specific surface area, thermal stability and electrical conductivity.[18]

Herein, an innovative label-free voltammetric aptasensor was fabricated for specific and ultrasensitive determination of LPS. Firstly, the PEI-rGO-MoS_2 nanocomposite was used as a nanocarrier to increase the loading of electroactive toluidine blue (TB). Then, gold nanoparticles (AuNPs) with a surface effect and good biocompatibility[19] were utilized to immobilize LBA and further amplify the electrochemical signal of TB. After the specific binding of LPS with LBA, the response signal from TB decreased with the increasing LPS concentrations, giving the quantitative foundation for LPS detection. The designed aptasensor showed satisfactory sensitivity, favorable specificity, and excellent stability, having possible applications in clinical testing.

2. Materials and methods

2.1. Reagents and materials

Endotoxin standard preparation, MoS_2 and TB were furnished from Sigma-Aldrich Chemical Co. (USA). Graphene oxide (GO) was purchased from Nanjing Xianfeng Nano Co. (Nanjing, China). Ethanol and trisodium citrate were supplied by Kelong (Chengdu, China). Dopamine (DA), ascorbic acid (AA), polyethyleneimine (PEI), chloroauric acid ($HAuCl_4$) and bovine serum albumin (BSA) were obtained from J&K Scientific Co., Ltd (Beijing, China). Healthy human sera were provided by the First Affiliated Hospital of Chongqing Medical University (Chongqing, China) and used for the spiked recovery of LPS. Regarding this issue, we state that the procedures followed are in accordance with the ethical standards of the Ethics Committee of Chongqing Medical University and with the Helsinki Declaration of 1975, as revised in 1983. The LBA with the sequence 5′-SH-$(CH_2)_6$-CTT CTG CCC GCC TCC TTC CTA GCC GGA TCG CGC TGG CCA GAT GAT ATA AAG GGT CAG CCC CCC AGG AGA CGA GAT AGG CGG ACA CT-3′[20] was synthesized and purified by Sangon Biological Engineering Technology Ltd (Shanghai, China).

20 mM TES buffer (pH 7.4) containing 10 mM Tris(2-carboxyethyl)phosphine hydrochloride, 1 mM EDTA and 0.1 mM NaCl was used to dissolve the thiolated LBA solution. The electrolyte solution of electrochemical impedance spectroscopy (EIS) was $Fe(CN)_6^{3-/4-}$ solution (5 mM) containing 0.1 M KCl. Phosphate buffer (0.1 M, pH 7.0) containing 10 mM KCl and 2 mM $MgCl_2$ was used for cyclic voltammetry (CV) measurement. All chemicals in this work were of analytical reagent grade and were not further processed. A Millipore Milli-Q purification system was used to prepare ultrapure water with a resistivity of 18.2 MΩ cm throughout the whole experiment.

2.2. Apparatus and measurements

All electrochemical measurements throughout the experiment were performed using a CHI660D electrochemical workstation (Shanghai Chenhua Instrument, China) in a three-electrode system consisting of a platinum wire as the auxiliary electrode, a saturated calomel electrode (SCE) as the reference electrode and a modified glass carbon electrode (GCE, 4 mm in diameter) as the working electrode. The morphological features were studied by field emission scanning electron microscopy (FESEM) (JSM7800F, Japan) and transmission electron microscopy (TEM) (H600, Hitachi Instrument, Japan). The elemental composition and structure of the prepared nanomaterials were confirmed by using Fourier-transform infrared (FTIR) spectroscopy (Thermo Nicolet, USA).

2.3. Preparation of the PEI-rGO-MoS_2 nanocomposite

Firstly, 10 mg GO was dissolved in 5 mL ultrapure water with vigorous sonication for 5 min to disperse it completely. Then, 1 mL of PEI (5%) solution was added dropwise into the GO solution under stirring for 30 min at room temperature. Subsequently, 5 mg MoS_2 was diluted in 2 mL of absolute ethanol with constant sonication for 5 min, followed by adding it into the above solution. After the mixture was heated in a water bath for 4 h at 90 °C, the product was centrifuged and washed several times with ultrapure water to remove excess reactant. Then, the obtained sediment was uniformly redissolved with 10 mL ultrapure water and stored in a refrigerator at 4 °C before use.

2.4. Preparation of AuNPs

The container was washed with a freshly prepared chromic acid solution before starting the preparation. Then 1 mL (1%) of $HAuCl_4$ was added to a vessel containing 100 mL of ultrapure water and heated until boiling. Subsequently, 2.5 mL (1%) trisodium citrate was rapidly added dropwise to the mixture. When the color changed from blue to red, it was con-

tinued to boil for 15 min. After cooling to room temperature, ultrapure water was added to the original volume to obtain a transparent burgundy liquid.[21]

2.5. Fabrication of the aptasensor

First, the GCE was polished with 0.3 μm and 0.05 μm alumina powder until the surface was smooth like a mirror. Then it was further electrochemically cleaned using a conventional method, followed by rinsing thoroughly with ultrapure water and drying in air. After that, 10 μL of PEI-rGO-MoS_2 solution was dropped on the pretreated electrode surface and dried in air. Subsequently, 8 μL TB solution was added to the electrode surface and incubated overnight at room temperature. After it was washed with ultrapure water, the modified electrode was soaked in AuNPs for 1 h. Then the electrode was incubated with LBA (2 μM) for 12 h and 10 μL BSA (3%) for 1 h to block excess binding sites. Finally, the modified GCE was soaked in a series of LPS solutions with different concentrations for 1 h at room temperature. Quantitative detection of LPS was performed based on the signal changes in the electrochemical response of TB before and after specific binding of LPS with LBA. The graphical representation of the stepwise construction process for the aptasensor is depicted in Fig. 1.

3. Results and discussion

3.1. Characterization of nanomaterials

The size and morphological feature images of the prepared nanomaterials were obtained by FESEM and TEM. It can be seen from Fig. 2A that rGO possessed a lamellar structure with folds. As shown in Fig. 2B, MoS_2 nanosheets illustrated a multi-layered sheet structure. The structural characterization indicated that the PEI-rGO-MoS_2 nanocomposite formed a broad sheet structure, and the single layers of MoS_2 nanosheets were uniformly covered on the surface of rGO (Fig. 2C). AuNPs exhibited a uniformly dispersed spherical structure with a diameter of about 15 nm (Fig. 2D).

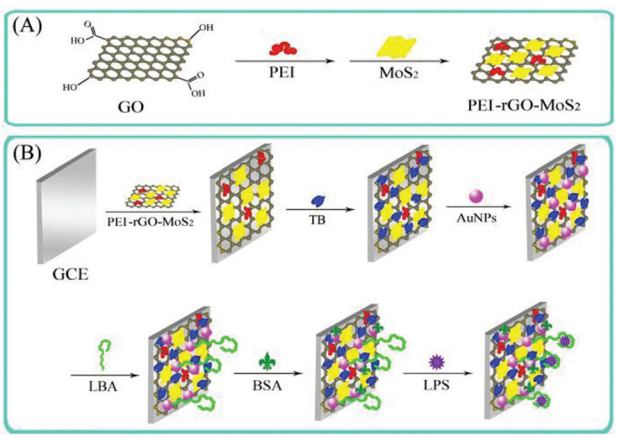

Fig. 1 (A) Illustration of the preparation of PEI-rGO-MoS_2. (B) Schematic diagram of the modification process of the aptasensor.

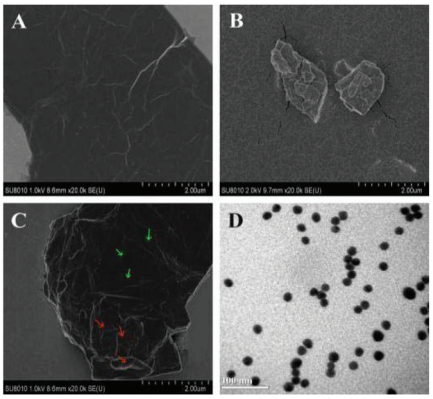

Fig. 2 FESEM images of (A) rGO nanosheets, (B) MoS_2, (C) the PEI-rGO-MoS_2 composite (red arrows point to MoS_2 and green arrows point to rGO nanosheets) and the TEM image of (D) AuNPs.

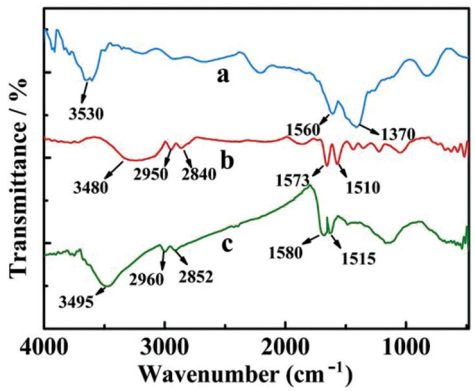

Fig. 3 FTIR spectra of (a) rGO, (b) PEI-rGO and (c) the PEI-rGO-MoS_2 nanocomposite.

Fig. 3 illustrates the spectra of rGO, PEI-rGO and PEI-rGO-MoS_2 obtained *via* FTIR spectroscopy. The broad absorption peak at 3530 cm^{-1} of the rGO (curve a) was attributed to the O–H stretching vibration of water molecules. The strong absorption peaks around 1560 and 1370 cm^{-1} corresponded to the –OH bond and C=C double bond, respectively.[22] The characteristic absorption peak of PEI-rGO (curve b) can be observed at about 2950 and 2840 cm^{-1}, which corresponds to the asymmetric and symmetric stretching vibrations of the $-CH_2-$ bonds of PEI.[23] Compared with the spectra of PEI-rGO, the absorption peaks of the methylene group, –OH bond and the C=C double bond of PEI-rGO-MoS_2 (curve c) were shifted to a high wavenumber.

3.2. Determination of the effective surface area of the aptasensor

The effective surface areas on different nanomaterial modified electrodes were calculated by carrying out CV measurement over a range of 0.02 to 0.2 V s^{-1} scan speeds (Fig. 4). The oxidation peak current (I_p) was a function of the square root of scan rate ($\nu^{1/2}$). The value of the effective area of the electrode

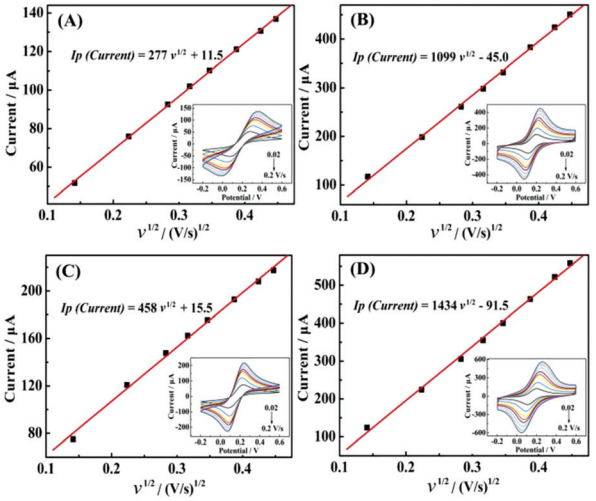

Fig. 4 The linear curves of oxidation peak current *vs.* square root of the scan rate for (A) bare GCE, (B) PEI-rGO/GCE, (C) MoS_2/GCE and (D) PEI-rGO-MoS_2/GCE in 5.0 mM $Fe(CN)_6^{3-/4-}$ solution at different scan rates ranging from 0.02 to 0.2 V s^{-1}. The insets illustrate the dependence of redox peak currents on different sweep rates taken from −0.20 to 0.60 V (*vs.* SCE).

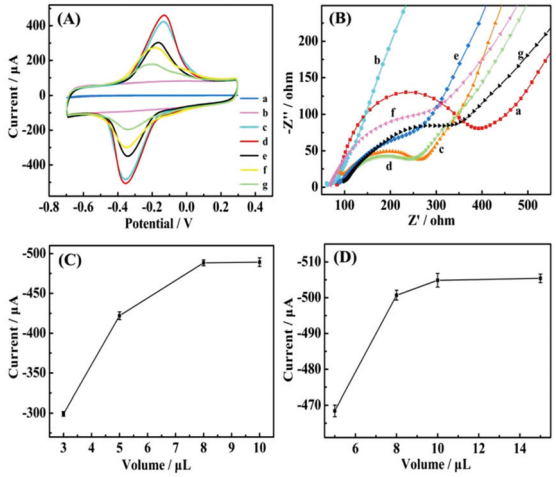

Fig. 5 CV responses (A) and EIS characterization (B) for each immobilization step: (a) bare GCE, (b) PEI-rGO-MoS_2/GCE, (c) TB/PEI-rGO-MoS_2/GCE, (d) AuNPs/TB/PEI-rGO-MoS_2/GCE, (e) LBA/AuNPs/TB/PEI-rGO-MoS_2/GCE, (f) BSA/LBA/AuNPs/TB/PEI-rGO-MoS_2/GCE and (g) LPS/BSA/LBA/AuNPs/TB/PEI-rGO-MoS_2/GCE. CVs were obtained from −0.70 to 0.30 V (*vs.* SCE) in 0.1 M phosphate buffer (pH 7.0) and EIS was performed in 5 mM $Fe(CN)_6^{3-/4-}$ electrolyte solution. Signal dependence of the different dosages of TB (C) and AuNPs (D). The error bars represent the results of standard deviations of three parallel measurements (n = 3).

was obtained according to the Randles–Sevcik equation: $I_p = 2.69 \times 10^5 \times n^{3/2} \times A \times D^{1/2} \times C \times \nu^{1/2}$, where ν is the scan rate, C is the concentration of the reactant in the bulk solution, D is the diffusion coefficient of the reactant, A is the effective surface area of the electrode, and n is the number of transfer electrons participating in the redox reaction (n = 1).[24]

The CV measurement was carried out at a scan rate of 100 mV s^{-1} in 5.0 mM $Fe(CN)_6^{3-/4-}$ solution, and the bare electrode, PEI-rGO, MoS_2 and PEI-rGO-MoS_2 modified electrodes exhibited an area of 7.95, 31.5, 13.2 and 41.2 mm^2, respectively. These results suggested that the PEI-rGO-MoS_2 nanocomposite can provide more binding sites for electroactive TB and significantly amplify the electrochemical detection signals of the aptasensor.

3.3. Electrochemical characterization of the aptasensor

CV measurement was used to investigate the electrochemical performance of the modified electrodes at each step of the manufacturing process (Fig. 5A). Compared with the bare GCE (curve a), the current response notably increased (curve b) after PEI-rGO-MoS_2 was modified on the GCE. When electroactive TB was immobilized on the electrode surface, a pair of obvious redox peaks were observed which were ascribed to the redox nature of TB (curve c). The redox peak generated from toluidine blue (TB) is mainly due to the reversible redox reaction between the reduced and oxidized forms of TB.[25] After the modified GCE was coated with AuNPs, the peak current was greatly amplified (curve d), due to the favorable biocompatibility and surface effect of AuNPs. It can be seen that the response decreased after incubating with LBA (curve e), because of the non-conductivity of the aptamer. When the excess AuNPs sites were blocked by BSA (curve f), the current value decreased again. After the target LPS (curve g) was modified on the GCE, the current further decreased as large proteins can significantly hinder the electron transfer.

EIS measurement was utilized to evaluate the interfacial characteristics of the aptasensor assembly process steps (Fig. 5B). The diameter of the semicircle in the high frequency region corresponded to the electron transfer resistance (R_{et}) in the electrode reaction. The bare GCE (curve a) revealed a R_{et} value of 305 Ω, while the impedance disappeared when the PEI-rGO-MoS_2 composite (curve b) was deposited on the GCE, mainly because the nanocomposite possessed excellent conductivity. After coating with TB (curve c), the value of R_{et} obviously increased to 275 Ω. The resistance slightly decreased to 250 Ω when AuNPs (curve d) were immobilized on the modified GCE, due to their ability to promote electron transfer. The value increased to 270 Ω after LBA (curve e) was dropped on the aptaelectrode and it can be ascribed to the inhibitory effect of the negative phosphate backbone on the electron flow. The impedance further increased to 295 Ω when BSA (curve f) was incubated onto the electrode on the basis of the insulating nature of protein macromolecules. After the surface-modified GCE was incubated with the LPS (curve g), the R_{et} value continued to increase to 350 Ω.

3.4. Optimization of the preparation conditions of the aptasensor

In order to achieve the optimal electrochemical analysis performance of the designed aptasensor, we assessed the influencing factors such as the dosages of TB (1.0 mg mL^{-1}) and AuNPs (0.10 mg mL^{-1}). As shown in Fig. 5C, the reduction

peak current response increased with increasing immobilization of TB modified on the electrode surface. It can be seen that the current continued to increase and tended to be flat at 8 μL. So, the optimal volume of TB was 8 μL. The volume of AuNPs was explored to achieve a more desirable signal amplification strategy. Fig. 5D reveals peak currents under different volumes of AuNPs. As the volumes of AuNPs increased from 5 μL to 10 μL, the reduction peak showed a continuous upward trend, and no longer rose when the volume reached 10 μL. Thus, 10 μL AuNPs were selected to modify the bioelectrode.

3.5. Performance of the aptasensor

3.5.1. Analytical performance of the aptasensor. The quantitative range of the fabricated aptasensor was verified by determining the various concentrations of the LPS standard solution using CV scanning under the optimized detection conditions. Fig. 6A illustrates the relationship between the addition of different concentrations of LPS and the electrochemical responses. With the increasing LPS concentrations, the current response of the biosensor decreased gradually in the range of 5.0×10^{-5} ng mL^{-1}–2.0×10^{2} ng mL^{-1}, owing to the blocking effect of biological macromolecules on electron transfer. The reduction peak current did not continue to change when the concentration was less than 5.0×10^{-5} ng mL^{-1} (curve c) compared to the incubation of 1.0×10^{-5} ng mL^{-1} LPS. As shown in Fig. 6B, the relationship between the logarithm of the LPS concentration and the reduction peak current can be observed. There was a good linear relationship in the range of 5.0×10^{-5} ng mL^{-1} to 2.0×10^{2} ng mL^{-1}, and the linear regression equation was $I = 7.77$ lgc-164. The LOD of the constructed aptasensor for LPS was appraised to be 3.01×10^{-5} ng mL^{-1} based on the $3\sigma/m$ criterion (where m is the slope of the calibration plot and σ is the standard deviation of the blank in the absence of the target). The rGO-MoS_2 with a large specific surface area and AuNPs with good biocompatibility endowed the aptasensor with excellent electrochemical detection behavior.

3.5.2. Specificity, stability and reproducibility of the aptasensor for LPS detection. LPS belongs to one of the composition of GNB cell wall, which is usually released and enters into the blood circulation after the lysis of bacteria. Therefore, the endogenous substances coexisting in the serum were utilized to assess the specificity and selectivity of the aptasensor, such as glucose (1 ng mL^{-1}), BSA (1 ng mL^{-1}), AA (1 ng mL^{-1}) and DA (1 ng mL^{-1}). Fig. 7A illustrates the histogram corresponding to the biosensor detecting target and different interferents. At the same concentration, LPS can significantly reduce the electrochemical response signal of the sensor compared to the interferents, exhibiting a satisfactory selectivity of the aptasensor for LPS detection.

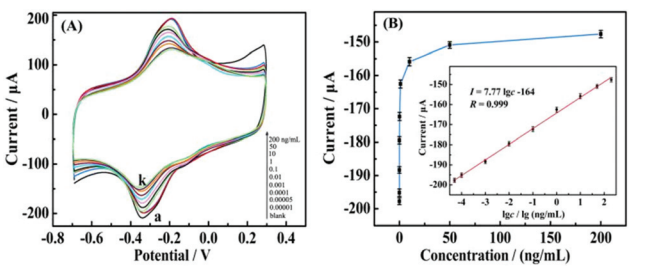

Fig. 6 (A) CV responses of the aptasensor with the addition of different concentrations of LPS standard solution in 0.1 M phosphate buffer (pH 7.0). (B) Response relationship between different LPS concentrations and the reduction peak current. The voltage at the peak current was −0.35 V. The inset demonstrates the calibration plot of LPS with the proposed aptasensor (n = 3).

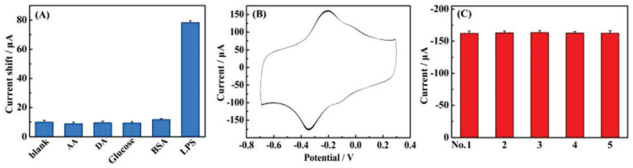

Fig. 7 (A) LPS (1 ng mL^{-1}) against the interferents (n = 3). (B) Stability of the aptasensor under successive CV scans for 50 cycles. (C) Current response of five different electrodes under the same optimal conditions (n = 3). CV scans were performed from −0.70 to 0.30 V with a scan rate of 0.1 V s^{-1} in 0.1 M phosphate buffer (pH 7.0).

Stability investigation of the aptasensor incubated with 10 pg mL^{-1} LPS was performed by taking successive CV scans for 50 cycles under the optimized conditions. When compared to the initial current response, the reduction peak current decreased only about 2.37% (Fig. 7B). The consequence revealed that the proposed aptasensor had favorable stability.

As shown in Fig. 7C, five equal electrodes incubated with the same concentration of LPS were analyzed to estimate the reproducibility of the aptasensor. When detecting 1 ng mL^{-1} LPS solution, the prepared aptasensors exhibited similar current response and the relative standard deviation (RSD) was 4.7%, suggesting that the aptasensor possessed an acceptable reproducibility.

In addition, we systematically compared the differences in the analysis performance between the fabricated aptasensor and other LPS test assays reported in the literature (Table 1). According to the results, it can be seen that the proposed sensor showed a wider linear range and a lower LOD for LPS detection. The advantage and novelty of the present work should be ascribed to the following aspects. First of all, the high affinity between the aptamer and LPS increases the specificity of the sensor. Additionally, the label-free aptasensor can simplify the operation sequence with fast response. Furthermore, the PEI-rGO-MoS_2 nanocomposite with a larger specific surface area, thermal stability and electrical conductivity amplifies the response signal and greatly increases the sensitivity of the sensor.

3.5.3. Application for the analysis of serum samples. When the host organism is infected by GNB, LPS release into the blood circulation. Therefore, human serum was chosen as the matrix for spiked recovery. In this work, a standard addition

Table 1 Detection performance compared with other methods of LPS determination

Detection method	Recognition elements	Linear range	LOD	Ref.
Sandwich ELISA	Antibodies	1.0×10^{2}–1.0×10^{5} ng mL^{-1}	100 ng mL^{-1}	26
Real-time PCR	Microbes	30–3.0×10^{6} cfu mL^{-1}	—	27
Fluorescent sensor	Peptide variants	—	150 nM	11
Screen-printed sensor	Enzymes	0.001–0.1 ng mL^{-1}	—	28
Aptasensor	Aptamers	5.0×10^{-5}–2.0×10^{2} ng mL^{-1}	3.01×10^{-5} ng mL^{-1}	This work

Table 2 Recovery results obtained from the LPS aptasensor in human serum (n = 3)

Added LPS (ng mL^{-1})	Found LPS[a] (ng mL^{-1})	Recovery (%)	Relative standard deviation (%)
1.0×10^{-4}	1.01×10^{-4}	101	3.76
2.0×10^{-1}	1.97×10^{-1}	98.5	4.41
2.0×10^{2}	2.06×10^{2}	103	4.69

[a] Calculated as a mean of three measurements.

method was used to evaluate the analytical reliability and feasibility of the clinical application of the aptasensor. The concentrations of diluted human serum samples spiked with LPS solution in the experiment were 1.0×10^{-4} ng mL^{-1}, 2.0×10^{-1} ng mL^{-1} and 2.0×10^{2} ng mL^{-1}. As illustrated in Table 2, the corresponding recoveries for three concentrations of LPS were 101%, 98.5% and 103%, and the RSD values were 3.76%, 4.41% and 4.69%, respectively. These results suggested that the aptasensor had potential application in the quantitative detection of LPS in human serum.

4. Conclusions

In this work, a relatively simple and highly sensitive aptasensor was constructed for LPS detection based on the amplification of a PEI-rGO-MoS_2 nanocomposite. The as-synthesized nanocomposite with a large specific surface area and high electrical conductivity can greatly increase the loading of electroactive TB and enhance the electrochemical signal, leading to trace detection of LPS with a LOD as low as 3.01×10^{-5} ng mL^{-1}. The excellent electrochemical properties of the PEI-rGO-MoS_2 nanohybrid allow it to be used as a matrix for the electrochemical detection of other targets. The designed aptasensor can overcome the shortcomings of conventional LPS detection techniques such as long time consumption, unsatisfactory sensitivity and poor specificity. In addition, according to the results of spiked recovery experiment, the aptasensor showed feasibility for LPS determination in real serum samples. Compared with the existing approaches, this assay method possessed a wider linear range, better reproducibility and stability, which may provide an effective means for accurate detection of LPS. We believe that the aptasensor can be further improved in terms of sensitivity, specificity and stability, as novel nanomaterials and sensor detection methods are explored.

Conflicts of interest

There are no conflicts to declare.

Acknowledgements

This work is supported by the National Natural Science Foundation of China (81601856), the Third Batch of Young Backbone Teachers Funding Program in Colleges and Universities of Chongqing City ([2016] No. 53) and the Funds for Young Science and Technology Talent Cultivation Plan of Chongqing City (cstc2014kjrc-qnrc00004).

Notes and references

1 S. Brosel-Oliu, D. Galyamin, N. Abramova, F. X. Muñoz-Pascual and A. Bratov, *Electrochim. Acta*, 2017, **243**, 142.
2 S. Voss, R. Fischer, G. Jung, K. H. Wiesmüller and R. Brock, *J. Am. Chem. Soc.*, 2007, **129**, 554.
3 R. E. Unger, K. Peters, A. Sartoris, C. Freese and C. J. Kirkpatrick, *Biomaterials*, 2014, **35**, 3180.
4 C. Y. Park, S. H. Jung, J. P. Bak, S. S. Lee and D. K. Rhee, *Biologicals*, 2005, **33**, 145.
5 W. Jonathan, D. Nathan, J. Hasan, V. Enric, V. Adie and F. Ken, *J. Inflammation*, 2016, **13**, 24.
6 L. S. Gu and C. Q. Hu, *Chin. J. Antibiot.*, 2005, **30**, 731.
7 M. S. Victoria, R. A. Orbegozo-Medina, R. Fernanda, P. Esperanza and F. M. Ubeira, *PLoS One*, 2016, **11**, e0156530.
8 A. P. Das, P. S. Kumar and S. Swain, *Biosens. Bioelectron.*, 2014, **51**, 62.
9 E. C. Dullah and C. M. Ongkudon, *Crit. Rev. Biotechnol.*, 2017, **37**, 251.
10 L. Bai, Y. Chen, Y. Bai, Y. Chen, J. Zhou and A. Huang, *Biomaterials*, 2017, **133**, 11; S. Song, L. Wang, J. Li, C. Fan and J. Zhao, *Trends Anal. Chem.*, 2008, **27**, 108.
11 W. Su, M. Lin, H. Lee, M. Cho, W. Choe and Y. Lee, *Biosens. Bioelectron.*, 2012, **32**, 32.
12 S. E. Kim, W. Su, M. Cho, Y. Lee and W. S. Choe, *Anal. Biochem.*, 2012, **424**, 12; L. Bai, Y. Chai, X. Pu and R. Yuan, *Nanoscale*, 2014, **6**, 2902.
13 J. Yang, M. Heo, H. J. Lee, S. M. Park, Y. K. Jin and H. S. Shin, *ACS Nano*, 2011, **5**, 8365.
14 P. A. Rasheed, T. Radhakrishnan, P. K. Shihabudeen and N. Sandhyarani, *Biosens. Bioelectron.*, 2016, **83**, 361.

15 C. N. Rao, K. Gopalakrishnan and U. Maitra, *ACS Appl. Mater. Interfaces*, 2015, **7**, 7809; W. Zhang, P. Zhang, Z. Su and G. Wei, *Nanoscale*, 2015, **7**, 18364.
16 S. Das, R. Ghosh, P. Routh, A. Shit, S. Mondal, A. Panja and A. K. Nandi, *ACS Appl. Nano Mater.*, 2018, **1**, 2306; W. Zhang, P. Zhang, Z. Su and G. Wei, *Nanoscale*, 2015, **7**, 18364.
17 P. Jing, H. Yi, S. Xue, Y. Chai, R. Yuan and W. Xu, *Anal. Chim. Acta*, 2015, **853**, 234.
18 K. Chang and W. Chen, *ACS Nano*, 2011, **5**, 4720; J. Li, W. Tang, H. Yang, Z. Dong, J. Huang, S. Li, J. Wang, J. Jin and J. Ma, *RSC Adv.*, 2013, **4**, 1988; J. H. Luo, B. L. Li, N. B. Li and H. Q. Luo, *Sens. Actuators, B*, 2013, **186**, 84.
19 C. Shan, H. Yang, D. Han, Q. Zhang, A. Ivaska and L. Niu, *Biosens. Bioelectron.*, 2010, **25**, 1070.
20 Y. J. Lee, S. R. Han, J. S. Maeng, Y. J. Cho and S. W. Lee, *Biochem. Biophys. Res. Commun.*, 2012, **417**, 414.
21 N. T. H. Lien, V. X. Hoa, V. T. T. Duong, N. V. Tinh and T. H. Nhung, *Commun. Phys.*, 2011, **21**, 321.
22 Y. Shan, H. Zhang and F. Zhang, *Chin. J. Appl. Chem.*, 2015, **32**, 837.
23 A. M. Şenol, Y. Onganer and K. Meral, *Sens. Actuators, B*, 2017, **239**, 343.
24 L. Bai, R. Yuan, Y. Chai, Y. Yuan, Y. Wang and S. Xie, *Chem. Commun.*, 2012, **48**, 10972.
25 D. R. Jeykumari and S. S. Narayanan, *J. Nanosci. Nanotechnol.*, 2007, **7**, 1824; H. You, L. Bai, Y. Yuan, J. Zhou, Y. Bai and Z. Mu, *Biosens. Bioelectron.*, 2018, **117**, 706.
26 Z. S. Zhou, Z. J. Luo and C. H. Hao, *J. Environ. Health*, 2012, **29**, 185.
27 A. A. Mafu, M. Pitre and S. Sirois, *J. Food Prot.*, 2009, **72**, 1310.
28 K. Y. Inoue, S. Takano, S. Takahashi, Y. Ishida, K. Ino, H. Shiku and T. Matsue, *Analyst*, 2013, **138**, 6523.